

Six-DOF Spacecraft Dynamics Simulator For Testing Translation and Attitude Control

Farhad Aghili*

Abstract

This paper presents a method to control a manipulator system grasping a rigid-body payload so that the motion of the combined system in consequence of external applied forces to be the same as another free-floating rigid-body (with different inertial properties). This allows zero-g emulation of a scaled spacecraft prototype under the test in a 1-g laboratory environment. The controller consisting of motion feedback and force/moment feedback adjusts the motion of the test spacecraft so as to match that of the flight spacecraft, even if the latter has flexible appendages (such as solar panels) and the former is rigid. The stability of the overall system is analytically investigated, and the results show that the system remains stable provided that the inertial properties of two spacecraft are different and that an upperbound on the norm of the inertia ratio of the payload to manipulator is respected. Important practical issues such as calibration and sensitivity analysis to sensor noise and quantization are also presented.

1 Introduction and Motivation

Ground testbed facilities have been used for spacecraft control hardware/software verification since various space programs began half a century ago [1–4]. Due to the high cost of launch and operations associated with on-orbit repair, a spacecraft must operate reliably once it is placed in orbit. Therefore, realistic testing of spacecraft prior to launch, ideally with all hardware/software in place, ought to be undertaken to ensure that the spacecraft functions as intended. One of the challenges of this approach is that testing must take place in a 1-g environment, whereas the actual system will eventually operate in a zero-g environment. This has motivated building of testbed facilities in various government and university laboratories for the analysis and testing of spacecraft.

Gas-jet thrusters and reaction/momentum wheels are commonly employed as actuators for spacecraft attitude and/or translation control [5]. Simulation is widely used for characterizing the functional behavior of spacecraft control systems [6, 7]. This approach may be inadequate and it should be highly desirable to be able to test and validate system performance based on the behavior of actual sensors and actuators, which are difficult to model [5, 8–10]. There are many technologies to address the problem of reproducing the micro-gravity space environment, such as air bearings, underwater test tanks, free-fall tests, and magnetic suspension systems. However,

*email: faghili@encs.concordia.ca

of these, only air bearings have proven useful for testing spacecraft. Achieving weightlessness by using natural buoyancy facilities, i.e., water tank, has been used extensively for astronaut training. However, a functional spacecraft can not be submerged in the water, and in addition viscous damping does not allow a perfect force-free environment. A free-fall test through flying parabolas in aircraft can achieve zero-g in a 3-D environment. But only for brief periods. Magnetic suspension systems provide only a low force-torque dynamic environment with a small range of motion. Air-bearing tables (also known as planar air-bearings) [11, 12] and spherical air-bearings [3] are commonly used for ground-based testbeds for testing the translation and attitude control systems of a spacecraft.

An emulation of zero-g translational motion can be achieved by an air-bearing table on which a spacecraft translates on a surface perpendicular to the gravity vector while being floated on a cushion of compressed air with almost no resistance. This technique has been used for testing various space systems such as formation flying [13, 14], free-flying space robots [15, 16], orbital rendezvous and docking [17, 18], capturing mechanisms of spacecraft [19, 20], and free-flying inspection vehicles [14, 21], and space robotics [4, 21–28]. Although the air-bearing table system can be utilized to test some physical components of spacecraft control systems including the sensors and actuators, this system is limited to a two-dimensional planar environment. Spherical air-bearings have been used for spacecraft attitude determination and control hardware/software verification for many years [3]. The earliest development and design of a satellite simulator based on spherical air-bearing with three axes of rotation was reported in [29], and has now evolved into modern testbed facilities [30–32]. A spherical air-bearing yields minimum friction and hence offers a nearly torque-free environment if the center of mass is coincident with the bearing’s center of rotation. The main problem with the air bearing system is the limited range of motion resulting from equipment being affixed to the bearing [32]. Also, spherical air-bearings are not useful for simulating spacecraft having flexible appendages, because the location of the center-of-mass of such spacecraft is not fixed. Although one can envisage combining the two air-bearing technologies in a testbed for reproducing both the rotational and translational motions, complete freedom in all six rigid degrees-of-freedom is still technically difficult to achieve [3].

Motion table testing systems allow the incorporation of real sensors of a satellite such as gyros and star trackers in Hardware-In-The-Loop (HIL) simulation loops. However, actuators such as reaction wheels or gas-jet thrusters have been simulated. The main idea in HIL simulation is that of incorporating a part of real hardware in the simulation loop during the system development [33]. Rather than testing the control algorithm on a purely mathematical model of the system, one can use real hardware in the simulation loop [2, 33]. This allows for detailed measurement for accurate performance assessment of the system under the test. The concept of the HIL methodology has also been utilized for design and implementation of various laboratory testbeds to study the dynamic coupling between a space-manipulator and its host spacecraft operating in free space [11, 34–43]. A system called the Vehicle Emulation System Model II (VES II) permits the experimental evaluation of planning and control algorithm for mobile terrestrial and space robot systems by using the so-called ”admittance control” [36]. Similar concepts have been also pursued by other space agencies such as DLR [44], NASA and CSA [10, 45–47] for different applications.

The existing impedance-controller based HIL simulators only compensate for the effect of gravity wrench on the force/moment measurement, while the effect of the payload’s inertial

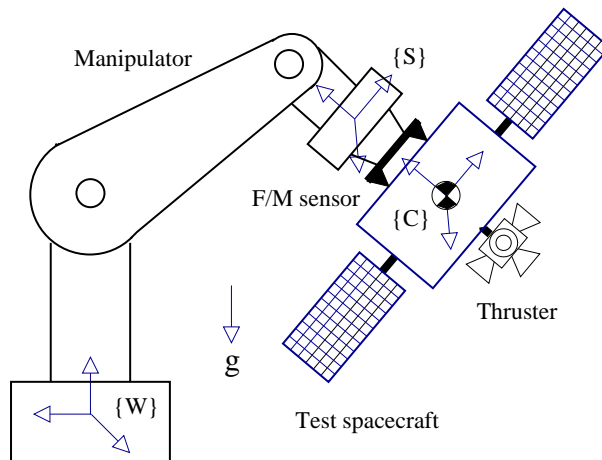


Figure 1: A ground spacecraft mounted on a manipulator.

forces (the test spacecraft in our case) has not been taken into account. Heavy payloads, however, not only changes the manipulator dynamics but also, incorporate significant inertial as well as gravitational force components into the measurement that can fail a conventional impedance controller to achieve the desired dynamics.

In this paper, we propose a method to control a manipulator with a heavy payload, e.g., a test spacecraft, so that the closed-loop system dynamics with respect to external force be as if the payload is with inertia properties corresponding to a flight spacecraft [1]. Fig. 1 schematically illustrates the test spacecraft, i.e., a scale model of the flight spacecraft, is rigidly attached to a manipulator arm. A six-axis force-moment sensor is installed at the interface of the spacecraft and the manipulator, for sensing the external forces – for instance, firing thrusters – superimposed by gravitational and inertial forces. Upon measurement of the wrist force-moment and the joint angles and velocities, the signals are used by a control system that moves the manipulator and the test spacecraft with it appropriately. Such a setup allows virtually testing the actual control system, electronics, sensors, and actuators of a spacecraft in a closed-loop configuration in the laboratory environment. The distinct contribution of this work is a control system which incorporates dynamics models of the test spacecraft (payload), flight spacecraft as well as the manipulator to accurately replicate the motion dynamics of the flight spacecraft using a scaled mockup, as presented in Section 2.2. Notably, the controller can compensate for the inertial forces of the payload without needing any acceleration measurement; this is not attainable with the conventional admittance controllers. A calibration procedure to precisely null out the static component of the F/M sensor in addition to sensitivity analysis are presented in Section 3. Section 4 is devoted to emulation of spacecraft having flexible appendages, e.g., solar panels.

2 Control System

2.1 Dynamics Model

The translational and the rotational motion dynamics of a *flight spacecraft* can be conveniently expressed in a body-fixed frame $\{C_s\}$ as

$$M_s \dot{\nu}_s + h_s(\nu_s) = \mathcal{F}_{\text{ext}}, \quad (1)$$

where

$$M_s = \text{diag}\{m_s I, I_{C_s}\}, \quad h_s(\nu_s) = \begin{bmatrix} m_s \omega_s \times v_s \\ \omega_s \times I_{C_s} \omega_s \end{bmatrix},$$

I denotes the identity matrix, m_s and I_{C_s} are the spacecraft mass and inertia tensor, $\nu_s^T = [v_s^T \ \omega_s^T]$ is the generalized velocity including the components of the linear velocity v_s and angular velocity ω_s of the spacecraft CM, and \mathcal{F}_{ext} is the generalized external forces (due to the spacecraft actuators, e.g., thrusters or reaction wheels). It is worth mentioning that estimation of the other sources of external forces and torques such as gravity gradient, thin-air drag, and solar pressure can be added to the right-hand side (RHS) of (1) to achieve a more accurate result.

Fig. 1 illustrates the *test spacecraft* held by a manipulator. The test spacecraft is of mass and inertia m_m and I_{C_m} , respectively, that are different from those of the flight spacecraft. The F/M sensor installed in the mechanical interface of the manipulator and the test spacecraft allows us to measure the force/moment interactions between the two systems. The coordinate-frame $\{W\}$ is fixed to the manipulator base and, the origin of body-fixed frame $\{C\}$ is chosen to be coincident with the CM of the test spacecraft, and its orientation with respect to frame $\{W\}$ is represented by the rotation matrix R . The test spacecraft is exposed to three different forces: the external force \mathcal{F}_{ext} , gravitational force \mathcal{F}_g , and force interaction between the test spacecraft and the manipulator \mathcal{F}_s that is measured by the F/M sensor. Note that \mathcal{F}_s is expressed in the body-fixed coordinate frame $\{S\}$ coincident with the sensor coordinate and parallel to $\{C\}$. Thus

$$\mathcal{F}_g = \begin{bmatrix} m_m g R^T k \\ 0 \end{bmatrix}, \quad (2)$$

where unit vector k is aligned with the gravity vector¹ which is expressed in the manipulator's base frame $\{W\}$, and $g = 9.81 \text{ m/s}^2$. Similar to (1), the dynamics of the test spacecraft can be described by

$$\begin{aligned} M_m \dot{\nu} + h_m(\nu) &= -T \mathcal{F}_s + \mathcal{F}_g + \mathcal{F}_{\text{ext}} \\ &= -\mathcal{F}_{sg} + \mathcal{F}_{\text{ext}}. \end{aligned} \quad (3)$$

where T denotes the transformation from frame $\{S\}$ to $\{C\}$, i.e.

$$T = \begin{bmatrix} I & 0 \\ -[c \times] & I \end{bmatrix}, \quad [c \times] = \begin{bmatrix} 0 & -c_z & c_y \\ c_z & 0 & -c_x \\ -c_y & c_x & 0 \end{bmatrix},$$

¹If the z-axis of the coordinate frame $\{W\}$ is perfectly parallel to the earth's gravity vector, then $k^T = [0 \ 0 \ -1]$.

vector c denotes the location of the center-of-mass and

$$\mathcal{F}_{sg} \triangleq T\mathcal{F}_s - \mathcal{F}_g. \quad (4)$$

2.2 Control Law

We assume that both the test and flight spacecraft experience the same actuation force \mathcal{F}_{ext} , and that their generalized velocities are the same, i.e., $\nu = \nu_s$. Under these assumptions, we can say the test spacecraft is dynamically equivalent to the flight spacecraft if they produce identical accelerations, i.e., $\dot{\nu} = \dot{\nu}_s$. However, the accelerations are governed by two different equations of motion, and hence, in general, $\dot{\nu} \neq \dot{\nu}_s$. Nevertheless, it is possible to achieve dynamical similarity if the manipulator is properly controlled. To this end, we define an estimation of the acceleration $\dot{\nu}^*$ that is obtained by subtracting (3) from (1), i.e.,

$$M_\Delta \dot{\nu}^* + h_\Delta = \mathcal{F}_{sg}, \quad (5a)$$

where

$$M_\Delta \triangleq \begin{bmatrix} (m_s - m_m)I & 0 \\ 0 & I_{C_s} - I_{C_m} \end{bmatrix}, \quad (5b)$$

$$h_\Delta \triangleq \begin{bmatrix} (m_s - m_m)\omega \times v \\ \omega \times (I_{C_s} - I_{C_m})\omega \end{bmatrix}. \quad (5c)$$

Assumption 1 *In the followings, we assume that M_Δ is a non-singular matrix, i.e.,*

$$m_s \neq m_m \quad \text{and} \quad \lambda_i(I_{C_s} - I_{C_m}) \neq 0 \quad \forall i = 1, \dots, 3. \quad (6)$$

Notice that $\dot{\nu}^*$ does not have any physical meaning, rather it is just a definition. Let $J = [J_v^T \ J_\omega^T]^T$ represent the manipulator Jacobian expressed in the coordinate frame $\{C\}$, where sub-matrices J_v and J_ω denote the translational and rotational Jacobians, respectively. That is $v(q, \dot{q}) = J_v \dot{q}$ and $\omega(q, \dot{q}) = J_\omega \dot{q}$, where q is the vector of joint angles. The time derivative of the velocity equation leads to

$$\dot{\nu} = J\ddot{q} + \dot{J}\dot{q}. \quad (7)$$

In view of equations (7) and (5a) and Assumption 1, we define \ddot{q}^* to be an estimation of the joint accelerations as

$$\ddot{q}^* \triangleq J^{-1}(\dot{\nu}^* - \dot{J}\dot{q}) \quad (8a)$$

$$= J^{-1}M_\Delta^{-1}\mathcal{F}_{sg} - J^{-1}(N + \dot{J})\dot{q}, \quad (8b)$$

with $M_\Delta^{-1}h_\Delta = N\dot{q}$ and

$$N(q, \dot{q}) \triangleq \begin{bmatrix} [J_\omega \dot{q} \times] J_v \\ (I_{C_s} - I_{C_m})^{-1} [J_\omega \dot{q} \times] (I_{C_s} - I_{C_m}) J_\omega \end{bmatrix}.$$

Note that (8b) is obtained assuming that kinematic singularity does not occur.

Assume that the manipulator dynamics are characterized by inertia matrix $M_r(q)$ and the nonlinear vector $h_r(q, \dot{q})$, which contains Coriolis, centrifugal and gravitational terms. One can show that the equations of motion of the combined system of the manipulator and the payload can be written in the standard form as:

$$M_t \ddot{q} + h_t(q, \dot{q}) = \tau + J^T \mathcal{F}_{\text{ext}} \quad (9a)$$

where τ denotes the joint torques, and

$$M_t(q) \triangleq J^T M_m J + M_r(q), \quad (9b)$$

$$h_t(q, \dot{q}) \triangleq h_r(q, \dot{q}) + J^T h_m(\dot{q}) + J^T M_m \dot{J} \dot{q} - m_m g J_v^T R^T k \quad (9c)$$

Now, the objective is to force the manipulator to follow the trajectory dictated by (8b). Although it seems that this goal can be achieved by using an inverse-dynamics controller [48–50] based on the manipulator dynamics, such a controller will lead to an algebraic loop that is not legitimate from the control point of view. Note that the force sensor signal contains components of the inertial forces due to the acceleration. Thus, compensating for \mathcal{F}_s results in a torque control law which has a direct component of the acceleration, while the acceleration is algebraically related to the joint torques. This problem can be alleviated by using an inverse-dynamics controller based on the complete model (9a) and by compensating for an estimation of the external force \mathcal{F}_{ext} . That is

$$\begin{aligned} \tau = & M_t(q) \ddot{q}^* + h_t(q, \dot{q}) - J^T \mathcal{F}_{\text{ext}}^* \\ & + M_t(q) \left(K_d \left(\int \ddot{q}^* dt - \dot{q} \right) + K_p \left(\int \int \ddot{q}^* dt - q \right) \right), \end{aligned} \quad (10)$$

with $K_d = k_d I$ and $K_p = k_p I$ being the controller gains and \mathcal{F}^* being an estimation of the external force. In the following analysis, we will show that the above inverse-dynamics controller in conjunction with a force estimator lead to exponential stability. Let $\ddot{q} \triangleq \ddot{q}^* - \ddot{q}$ denotes the joint acceleration error, then the corresponding Cartesian acceleration error is readily obtained from definition (8a) as

$$\dot{\tilde{v}} \triangleq \dot{v}^* - \dot{v} = J(q) \ddot{q}. \quad (11)$$

Substitution of \dot{v}^* obtained from (5a) into the above equation yields

$$\dot{v} = M_{\Delta}^{-1} \mathcal{F}_{sg} - N \dot{q} - J \ddot{q}.$$

Now, upon substitution of the acceleration from the above into (3), we can write the expression of the external force as:

$$\mathcal{F}_{\text{ext}} = \mathcal{F}_{\text{ext}}^* + \tilde{\mathcal{F}}_{\text{ext}},$$

where

$$\mathcal{F}_{\text{ext}}^* = (I + M_m M_{\Delta}^{-1}) \mathcal{F}_{sg} + h_m - M_m N \dot{q} \quad (12)$$

is the estimation of the external force and

$$\tilde{\mathcal{F}}_{\text{ext}} = -M_m J \ddot{q} \quad (13)$$

is the force estimation error. Clearly, the force estimation error goes to zero only if the acceleration error does so. We will show that under a mild condition, controller (10) in conjunction

with force estimator (12) results in exponential stabling of the motion and force errors. To this end, substitution of $\mathcal{F}_{\text{ext}}^*$ and \ddot{q}^* obtained from (12) and (8b), respectively, into (10) yields the expression of the control law as:

$$\begin{aligned} \tau = & J^T (M_{Cr}(q)M_{\Delta}^{-1} - I)\mathcal{F}_{sg} + h_r(q, \dot{q}) - M_r(q)J^{-1}(N(q, \dot{q}) + \dot{J})\dot{q} \\ & - m_m g J_v^T R^T k + M_t(q) \left(K_d \left(\int \ddot{q}^* dt - \dot{q} \right) + K_p \left(\int \int \ddot{q}^* dt - q \right) \right), \end{aligned} \quad (14)$$

where $M_{Cr} \triangleq J^{-T} M_r J^{-1}$ is the *Cartesian inertia* of the manipulator. Stability of closed-loop system remains to be proved. Knowing that (14) becomes equivalent to (12) if the force term, \mathcal{F}_{ext} , of the former equation is replaced by $\mathcal{F}_{\text{ext}}^* = \mathcal{F}_{\text{ext}} - \tilde{\mathcal{F}}_{\text{ext}}$, we can arrive at the equations of the motion and force errors by substituting (14) into system (9a), i.e.,

$$M_t(\ddot{\tilde{q}} + K_d \dot{\tilde{q}} + K_p \tilde{q}) = -J^T \tilde{\mathcal{F}}_{\text{ext}}.$$

Moreover, we know that the force and acceleration errors are related by (13). Thus

$$M_r \ddot{\tilde{q}} + M_t(K_d \dot{\tilde{q}} + K_p \tilde{q}) = 0,$$

which can be rewritten as:

$$\ddot{\tilde{q}} + K_d \dot{\tilde{q}} + K_p \tilde{q} + Q(q)(K_d \dot{\tilde{q}} + K_p \tilde{q}) = 0, \quad (15)$$

where

$$Q \triangleq M_r^{-1}(JM_m J^T). \quad (16)$$

We will show that system (15) remains stable if the coefficient matrix of the additive term, Q , is sufficiently small. Let assume that $x^T = [\tilde{q}^T \quad \dot{\tilde{q}}^T]$ represent the state vector. Then, (15) can be written as

$$\dot{x} = Ax + \epsilon(t, x) \quad (17)$$

where

$$A = \begin{bmatrix} 0 & I \\ -K_p & -K_d \end{bmatrix} \quad \text{and} \quad \epsilon(t, x) = -Q \begin{bmatrix} 0 \\ K_p \tilde{q} + K_d \dot{\tilde{q}} \end{bmatrix}.$$

Since the perturbation term ϵ satisfies the linear growth bound

$$\|\epsilon\| \leq \sqrt{k_p^2 + k_d^2} \|Q\| \|x\|,$$

system (17) is in the form of *vanishing perturbation* [51]. Moreover, since A is Hurwitz, there exists Lyapunov function

$$V(x) = x^T P x \quad (18)$$

with $P > 0$ satisfying

$$PA + A^T P = -I. \quad (19)$$

The derivative of $V(x)$ along trajectories of perturbed system (17) satisfies

$$\dot{V} \leq (-1 + 2\sqrt{k_p^2 + k_d^2} \lambda_{\max}(P) \|Q\|) \|x\|^2 \quad (20)$$

On the other hand, the solution of the Lyapunov equation (19) is given by

$$P = \frac{1}{2k_p k_d} \begin{bmatrix} k_p(k_p + 1) + k_d^2 & k_d \\ k_d & k_p + 1 \end{bmatrix},$$

which verifies

$$\lambda_{\max}(P) \leq \frac{(k_p + 1)^2 + k_d^2}{2k_p k_d}.$$

Therefore, according to the stability theorem of perturbed system [51, p. 206], the origin of (17) is globally exponentially stable if

$$\|Q\| \leq \alpha(k_p, k_d) = \frac{k_p k_d}{((k_p + 1)^2 + k_d^2)^{\frac{3}{2}}}. \quad (21)$$

Using the norm properties in (16), we obtain a conservative condition for the stability as:

$$\lambda_{\max}(M_m) \leq \alpha(k_p, k_d) \frac{\lambda_{\min}(M_r)}{\lambda_{\max}(J J^T)}. \quad (22)$$

Now, if (21) is satisfied, then there must exist scalar $\Omega > 0$ such that $\|x\| \leq \|x(0)\|e^{-\Omega t}$. Therefore, it can be inferred from (15) that

$$\|\ddot{q}\| \leq a e^{-\Omega t}, \quad (23)$$

where $a = (k_p^2 + k_d^2)(1 + \|Q\|)\|x(0)\|$.

Now, we are ready to derive the input/output relation of the closed loop system under the proposed control law. Adding both sides of (3) and (5a) yields

$$M_s \dot{\nu} + M_{\Delta} \dot{\nu}^* + h_s = \mathcal{F}_{\text{ext}}. \quad (24)$$

Finally, using (11) in (24), the equations of motion of the test spacecraft become

$$M_s \dot{\nu} + h_s(\nu) = \mathcal{F}_{\text{ext}} + \delta, \quad (25a)$$

where

$$\delta(t) = M_{\Delta} J \ddot{q} \quad (25b)$$

is a non-vanishing perturbation. Since J is always a bounded matrix, we can say

$$\sigma = \max_q \sqrt{\lambda_{\max}(J^T J)},$$

where $\lambda_{\max}(\cdot)$ denotes the maximum eigenvalue of a matrix. It follows from (23) and (25b) that

$$\|\delta\| \leq \sigma a \lambda_{\max}(M_{\Delta}) e^{-\Omega t}, \quad (26)$$

which means that the perturbation exponentially relaxes to zero from its initial value. The above development can be summarized in the following.

Proposition 1 *Let a rigid-body object with generalized inertia M_m attached to a manipulator with inertia M_r . Assume that the force/moment developed at the interface of the object and the manipulator is sensed and fed back to the manipulator according to the control law (14). Moreover, assume that (6) and (21) are satisfied. Then, the motion of the object in response to external force \mathcal{F}_{ext} obeys equation of motion of another rigid-body object characterized by generalized inertia M_s .*

2.3 Force Feedback Gain

Ideally, the controller of the emulating system can change the inertia of the test spacecraft to any desired value. However, there are constraints (6) and (22) on the inertia matrices of the test and flight spacecraft as well as the manipulator that must be considered in the design. Assuming a steady-state mode in which the control error reaches zero, we can express the torque-control input by

$$\tau = J^T(M_{Cr}M_{\Delta}^{-1} - I)\mathcal{F}_{sg} + \eta(q, \dot{q}), \quad (27)$$

where $\eta(q, \dot{q})$ represents the motion dependent portion of the feedback, while the first term in the RHS of equation (27) is force feedback. In the following we examine two extreme cases of the force feedback gain.

2.3.1 Zero Gain

Equation (27) implies that the force feedback is disabled if $M_{Cr} = M_{\Delta}$ or

$$M_{Cr}(q) + M_m = M_s. \quad (28)$$

Clearly, to implement the emulation controller without force feedback requires satisfying (28) for all possible postures. However, with the exception of Cartesian manipulators, most manipulators are of configuration-dependent inertia matrix, whereas the spacecraft inertia are constant matrices. This means that the condition (28) can be satisfied only for few isolated postures at best. It is worth mentioning that the case of $M_s = M_m$ becomes a favorable condition if $M_{Cr} \equiv 0$, i.e., the manipulator inertia is negligible; see (28). However, a manipulator with zero mass (and zero joint friction) can be thought of as an air-bearing simulator system, which has its own shortcomings as described in Section 1.

2.3.2 Infinite Gain

It is apparent from (27) that for the control torque effort to be bounded requires that M_{Δ} be a non-singular matrix, i.e., condition (6) is satisfied. At first glance, this result seems counterintuitive. But, it can be seen from (5a) that the acceleration and thus the subsequent motion trajectory can be uniquely estimated only if M_{Δ} is a full-rank matrix. It is also apparent from (1) and (3) that the only possibility for the flight and test spacecraft with the same mass and inertia to produce similar velocity and acceleration trajectories with respect to external force \mathcal{F}_{ext} is that the interaction force \mathcal{F}_{sg} becomes zero. Clearly, in such a case, it is not possible to predict the position and velocity trajectories from the estimated acceleration and hence the feedback is meaningless.

3 Simulating a Micro-G Environment

3.1 Precise Gravity Compensation

Performing a high-fidelity zero-g emulation critically relies on a precise force/moment feedback which, in turn, is determined by: (i) Accuracy of the gravity compensation; (ii) the resolution of the F/M sensor. These issues are discussed below.

3.1.1 Calibration

The static components of the F/M sensor output include the sensor offset and the payload gravitational force, which are not distinguishable from each other. Nevertheless, if a sequence of sensor readings is recorded by locating the manipulator in several known poses, it is possible to identify the sensor offset together with all the gravity parameters that are required to null out the static components of the sensor.

If the gravity were completely compensated, then for every position we would have $\mathcal{F}_{sg} = 0$, i.e., $T(\mathcal{F}_s - \mathcal{F}_0) - \mathcal{F}_g = 0$, where $\mathcal{F}_0^T = [f_0^T \ n_0^T]$ denotes the sensor offset. Now, we consider $\{\mathcal{F}_0, m_m, c, k\}$ as the set of uncertain parameters that are to be identified. Defining vector $w \triangleq m_m k$ and knowing that $[c \times] R^T w = -[(R^T w) \times] c$, we can break up $\mathcal{F}_s = T^{-1} \mathcal{F}_g + \mathcal{F}_0$ into two *linear regression* equations as

$$f_s = [I \quad gR^T] \begin{bmatrix} f_0 \\ w \end{bmatrix}, \quad (29a)$$

$$n_s = [I \quad -gm_m[(R^T k) \times]] \begin{bmatrix} n_0 \\ c \end{bmatrix}, \quad (29b)$$

where $\mathcal{F}_s^T = [f_s^T \ n_s^T]$. Now stacking p measurements $y_1^T = [f_{s1}^T, f_{s2}^T, \dots, f_{sp}^T]$ and $y_2^T = [n_{s1}^T, n_{s2}^T, \dots, n_{sp}^T]$, that are obtained by configuring the manipulator at p different positions $\{q_1, q_2, \dots, q_p\}$, we can derive two linear matrix relations $y_1 = \Psi_1(q)\Theta_1$ and $y_2 = \Psi_2(q, \Theta_1)\Theta_2$ from (29a-29b), where vectors Θ_1 and Θ_2 contain the parameters of interest. Finally, assuming a sufficient number of independent equations, one can obtain the vectors of estimated parameters $\hat{\Theta}_1$ and $\hat{\Theta}_2$ consecutively by using the least squares method from

$$\hat{\Theta}_1 = \Psi_1^+ y_1, \quad \text{and} \quad \hat{\Theta}_2 = \Psi_2^+(\hat{\Theta}_1) y_2,$$

where $\Psi_i^+ = \Psi_i^T (\Psi_i \Psi_i^T)^{-1}$ is the pseudo-inverse of Ψ_i . Note that the mass and the gravitational vector can be retrieved from

$$\hat{m}_m = \|\hat{w}\| \quad \text{and} \quad \hat{k} = \frac{\hat{w}}{\|\hat{w}\|}.$$

3.1.2 Position Errors and Accuracy of the Gravity Compensation

Error between the measured joint angles used by the gravity compensator and the true joint angles will result in a small residual static force acting on the payload. One source of this error is measured quantization. In order to minimize the residual force induced by the quantization as much as possible, we need to employ high-resolution encoders at the joints so that the induced error becomes at least comparable to the F/M sensor resolution. In the following we relate the errors in the gravity compensation and the that of joint angles.

Assume that Δq and Δf_s denote small errors in measured joint angles and the computed gravity force, respectively. Using the Taylor series of (29a) leads to

$$\|\Delta f_s\| \leq gm_m \left\| \frac{\partial}{\partial q} R^T(q)k \right\| \|\Delta q\|. \quad (30)$$

Using the facts that all elements of the rotation matrix are sinusoidal functions of q and that k is a unit vector, one can show that a conservative bound on the first norm of the RHS of (30) is 6. Thus, a bound on the force error can be found as

$$\|\Delta f_s\| \leq 6gm_m\|\Delta q.\| \quad (31)$$

Similar argument shows that a conservative bound on the magnitude of moment error Δn_s can be found as

$$\|\Delta n_s\| \leq 6gm_m\|c\|\|\Delta q.\| \quad (32)$$

3.2 Assessing the Quality of the Micro-Gravity Environment

Emulation in a zero-gravity environment requires the static component of the F/M sensor is perfectly nulled out. However, in practice, this requirement can not be completely satisfied due to errors. A natural question rises; what is the quality of the emulator in simulating a weightlessness environment? To answer this question, let us assume that $\delta \bar{f}_{sg}$ denote the average magnitude error of the compensated F/M sensor output over several payload static poses. Then, the average acceleration introduced to the emulating system can be simply obtained by dividing the magnitude of this force by the inertia of the spacecraft being simulated. Normalizing the acceleration w.r.t. the Earth gravity constant, we define the following dimensionless index

$$\gamma \triangleq \frac{\delta \bar{f}_{sg}}{gm_s} \times 10^6 = \frac{\|\sum_i^n f_{s_i} - \Psi_{1_i} \hat{\Theta}_1\|}{ngm_s} \times 10^6 \quad (33)$$

to measure the virtual gravity of the simulated environment. In other words, the payload (test spacecraft) experiences as though it moves under a gravitational field with intensity of $\gamma \cdot g$ rather than a zero-g environment. It is worth pointing out that γ can be also interpreted as the drift exhibited by the emulation system. Similarly, the micro-gravity environment for the rotational motion can be defined as

$$\frac{\|\sum_i^n n_{s_i} - \Psi_{2_i} \hat{\Theta}_2\|}{ng\|c\|m_m} \times 10^6.$$

3.2.1 Resolution of F/M Sensor

At best, the force error $\delta \bar{f}_{sg}$ can be reduced down to the resolution of the F/M sensor. The resolution of a F/M sensor depends on its sensing range; a sensor with large sensing range tends to have lower resolution and vice versa. Since the F/M sensor is located at the manipulator-payload interface, the sensor should be selected so that its sensing range matches the weight of payload, i.e., the test spacecraft. Therefore, the ratio of the sensor resolution to its sensing range is the emulation system limitation in achieving the lowest micro-g.

Fig. 2 illustrates the best achievable micro-g's versus different spacecraft masses that is calculated from the resolutions and the sensing ranges of the commercial ATI F/M sensors [52]. Here, we assume that the scaling factor of the emulated spacecraft is two. It is evident from the figure that in the emulation of small to medium size spacecraft with mass of up to 500kg, the sensor resolution is sufficient for achieving accuracy of $16 \times 10^{-6}g$ (it almost remains constant

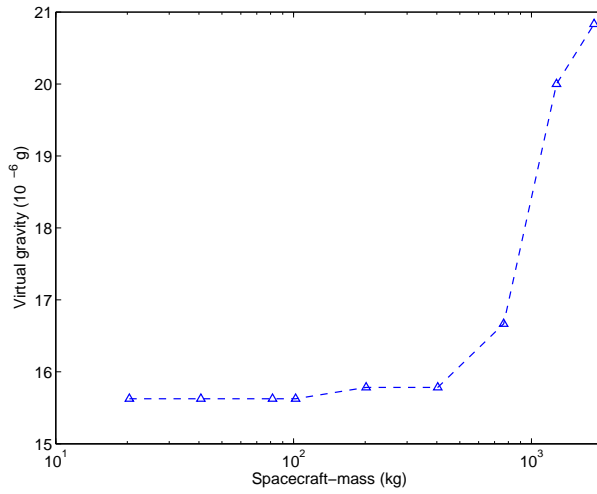


Figure 2: The best achievable micro-g environment, computed from the resolutions of a series of commercial F/M sensors, for emulation of spacecraft with different masses.

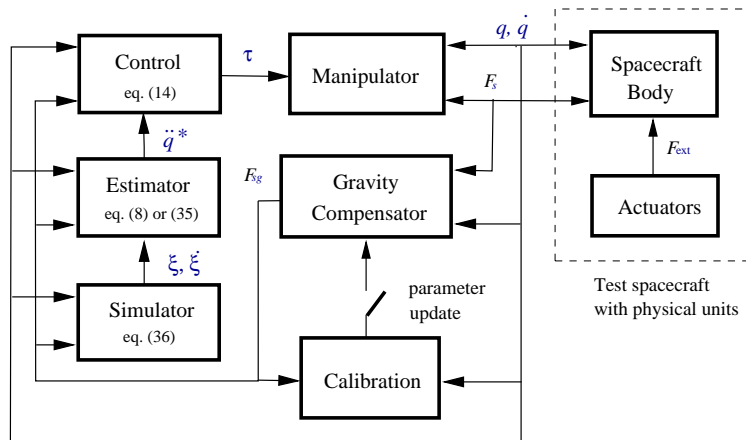


Figure 3: Architecture of the ground testbed for emulation of spacecraft.

in that range). However, the value of the virtual gravity dramatically increases, when the spacecraft mass exceeds that critical mass. This is due to the fact that commercial F/M sensors with large load capacity come with relatively low resolution. In order to improve the γ factor, one may use a mechanism to counter the effects of gravity in rigid-bodies [53–56]. For example, using a passive counterweight [53] can substantially reduce the static load on the F/M sensor, thereby allowing smaller and more precise sensor to be selected. The main disadvantage of this method is introduction of additional inertia. However, this is not an issue here because the controller can scale the inertia of the payload down or up to any desired value.

4 Emulation of Flexible Spacecraft

Many spacecraft have flexible appendages, e.g. satellites with solar panels, that can significantly affect their dynamics. However, testing a flexible spacecraft in a 1-g environment poses many

difficulties due to large deformation induced by gravity. Indeed, the structure of a solar panel cannot even hold itself against gravity when it is fully deployed. Moreover, the location of the CM of a flexible spacecraft is no longer fixed as it depends on the flexural coordinates whose direct measurement is not usually available. In the following, we extend the emulation concept for the case where the test spacecraft is rigid while the target flight spacecraft is flexible. It is assumed that the actuators are mounted to the rigid part of the test spacecraft. The test spacecraft lacks any flexible hardware, such as solar panels. Yet, motion perturbation caused by the flexible appendages is generated by simulation and then superimposed on the trajectories that subsequently drive the manipulator.

Let ξ denote the flexural coordinates of a flexible spacecraft. Then, the equations of motion for the entire system can be written in the partitioned mass matrix form

$$\begin{bmatrix} M_s & M_{sf} \\ M_{sf}^T & M_f \end{bmatrix} \begin{bmatrix} \dot{\nu} \\ \dot{\xi} \end{bmatrix} + \begin{bmatrix} h_{sr}(\nu, \xi, \dot{\xi}) \\ h_{sf}(\nu, \xi, \dot{\xi}) \end{bmatrix} = \begin{bmatrix} \mathcal{F}_{\text{ext}} \\ 0 \end{bmatrix}, \quad (34)$$

where M_f is the flexural inertia matrix, M_{sf} is the cross inertia matrix, h_{sr} and h_{sf} are the nonlinear vectors associated with the rigid and flexural coordinates. Analogous to the case of rigid spacecraft, subtracting equation (34) from (3) eliminates \mathcal{F}_{ext} from the equations of motion. Defining $\bar{M}_\Delta = M_\Delta - M_{sf}M_f^{-1}M_{sf}^T$ and $h_\Delta = h_{sr} - h_m$, we can write the accelerations of the rigid and the flexural coordinates by

$$\ddot{q}^* = -J^{-1}(N + J)\dot{q} - J^{-1}\bar{M}_\Delta^{-1}M_{sf}M_f^{-1}h_{sf} + \bar{M}_\Delta^{-1}\mathcal{F}_{sg}, \quad (35)$$

and

$$\ddot{\xi} = -M_f^{-1}(I + M_f^{-1}M_{sf}^T M_{sf}M_f^{-1})h_{sf} - M_f^{-1}M_{sf}^T\bar{M}_\Delta^{-1}(\mathcal{F}_{sg} - h_\Delta). \quad (36)$$

Equation (35) can be substituted in (14) to obtain the control law. However, to calculate the acceleration from (35) requires the value of the flexural states because h_{sr} and h_{sf} are functions of ξ and $\dot{\xi}$. An estimation of the flexural states can be obtained by simulation. First, the acceleration of the flexural coordinate can be computed by making use of the acceleration model (36), and then the flexural states are obtained as a result of numerical integration.

The architecture of the zero-g emulating testbed for spacecraft is illustrated in Fig. 3. To summarize, the emulation of flexible spacecraft may proceed as the following steps:

- i. start at a time when all of the system states, i.e., $\{q, \dot{q}, \xi, \dot{\xi}\}$ are known,
- ii. estimate the joint acceleration from (35) (use (8b) instead for rigid spacecraft),
- iii. apply control law (14) to the manipulator;
- iv. obtain the flexural states as a result of the consecutive integration of the acceleration obtained from (36) – skip this step for rigid spacecraft – and then go to step ii.

5 Conclusions

A control system for a manipulator carrying a rigid-body payload has been developed in order to modify the motion dynamics of the combined system in consequence of external according

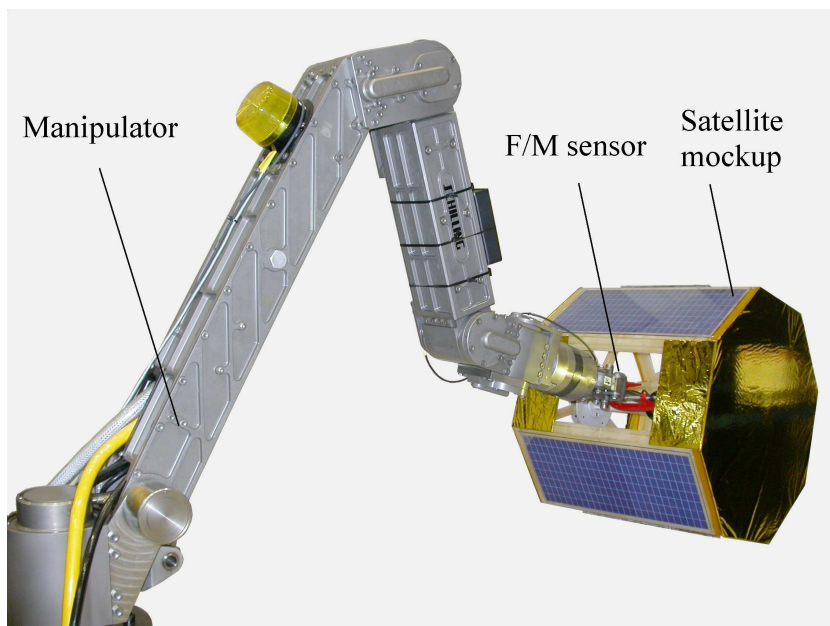


Figure 4: The spacecraft simulator using actively controlled manipulator.

to that of a free-floating body which has different inertial properties from the payload. This allowed zero-g emulation of the scaled prototype of a spacecraft (with non-negligible inertia) in a 1-g laboratory environment. It was shown that the controller in conjunction with the motion and force estimators could drive the manipulator so as to achieve dynamical similarity between the test and flight spacecraft. Notably, the controller can compensate for the inertial forces of the heavy payload (test spacecraft) without needing any acceleration measurement.

The stability of the closed loop system was analytically investigated. The results showed that system remains stable provided that mass and inertia of the test and flight spacecraft are not the same and that the norm of the inertia ratio of the payload to manipulator is upper bounded by a scalar which is a function of the controller gains. Finally, the methodology was extended for emulation of spacecraft having flexible appendages, e.g. solar panels.

A calibration procedure to precisely null out the static component of the F/M sensor was developed that tunes the gravity, kinematic, and sensor parameters all together. A sensitivity analysis showed that the position and force sensors have to be with specified resolutions in order to achieve a certain level of micro-gravity.

References

- [1] F. Aghili and M. Namvar, “Scaling inertia properties of a manipulator payload for 0-g emulation of spacecraft,” *The International Journal of Robotics Research*, vol. 28, no. 7, pp. 883–894, July 2009.
- [2] F. Aghili, M. Namvar, and G. Vukovich, “Satellite simulator with a hydraulic manipulator,” in *IEEE Int. Conference on Robotics & Automation*, Orlando, Florida, May 2006, pp. 3886–3892.

- [3] J. L. Schwartz, M. A. Peck, and C. D. Hall, “Historical review of air-bearing spacecraft simulators,” vol. 26, no. 4, pp. 513–522, 2003.
- [4] J.-C. Piedbœuf, J. de Carufel, F. Aghili, and E. Dupuis, “Task verification facility for the Canadian special purpose dextrous manipulator,” in *IEEE Int. Conf. on Robotics & Automation*, Detroit, Michigan, May 10–15 1999, pp. 1077–1083.
- [5] M. D. Griffin and J. R. French, *Space Vehicle Design*. SW, Washington, DC: AIAA, Inc., 1991.
- [6] W. E. Wiesel, *Spaceflight Dynamics*. New York: McGraw-Hill, 1989.
- [7] W. T. Thomson, *Introduction to Space Dynamics*. NY: Dover Publication, 1986.
- [8] J. R. Wertz, *Spacecraft Attitude Determination and Control*. Dordrecht, Netherlands: Kluwer, 1978.
- [9] F. Aghili, “Cartesian control of space manipulators for on-orbit servicing,” in *AIAA Guidance, Navigation and Control Conference*, Toronto, Canada, August 2010.
- [10] F. Aghili and K. Parsa, “An adaptive vision system for guidance of a robotic manipulator to capture a tumbling satellite with unknown dynamics,” in *IEEE/RSJ Int. Conf. on Intelligent Robots and Systems*, Nice, France, September 2008, pp. 3064–3071.
- [11] K. Yoshida, “Experimental study on the dynamics and control of a space robot with the experimental free-floating robot satellite (EFFORTS) simulator,” *Advanced Robotics*, vol. 9, no. 6, pp. 583–602, 1995.
- [12] F. Aghili, “A robotic testbed for zero-g emulation of spacecraft,” in *IEEE/RSJ Int. Conference on Intelligent Robots and Systems*, Edmonton, Alberta, Canada, 2005, pp. 1033–1040.
- [13] T. Corrazzini, A. Robertson, J. C. Adams, A. Hassibi, and J. P. How, “Experimental demonstration of GPS as a relative sensor for formation flying,” *Navigation: Journal of the Institute of Navigation*, vol. 45, no. 3, pp. 195–207, 1996.
- [14] H. Choset and D. Kortenkamp, “Path planning and control for free-flying inspection robot in space,” *Journal of Aerospace Engineering*, vol. 12, no. 2, pp. 74–81, 1999.
- [15] H. Schubert and J. How, “Space construction: An experimental testbed to develop enabling technologies IEEE,” in *Proceedings of the Conference on Telem manipulator and Telepresence Technologies IV*, Piscataway NJ, 1997, pp. 179–188.
- [16] F. Aghili, “Integrating IMU and landmark sensors for 3D SLAM and the observability analysis,” in *Proc. of IEEE/RSJ International Conference on Intelligent Robots and Systems (IROS)*, Taipei, Taiwan, Oct. 2010, pp. 2025–2032.
- [17] S. Matunaga, K. Yoshihara, T. Takahashi, S. Tsurumi, and K. Ui, “Ground experiment systems for dual-manipulator-based capture of damaged satellites,” in *IEEE Int. Conference on Intelligent Robots and Systems*, Piscataway, 2000, pp. 1847–1852.

- [18] F. Aghili, “Active orbital debris removal using space robotics,” in *International Symposium on Artificial Intelligence, Robotics and Automation in Space i-SAIRAS*, Turin, Italy, Sep. 4–6 2012.
- [19] S. Kawamoto, K. Matsumoto, and S. Wakabayashi, “Ground experiment of mechanical impulse method for uncontrollable satellite capturing,” in *Proceeding of the 6th Int. Symposium on Artificial Intelligence and Robotics & Automation in Space: I-SAIRAS*, St-Hubert, Canada, 2001.
- [20] F. Aghili, “A prediction and motion-planning scheme for visually guided robotic capturing of free-floating tumbling objects with uncertain dynamics,” *IEEE Transactions on Robotics*, vol. 28, no. 3, pp. 634–649, June 2012.
- [21] F. Aghili and K. Parsa, “Adaptive motion estimation of a tumbling satellite using laser-vision data with unknown noise characteristics,” in *2007 IEEE/RSJ International Conference on Intelligent Robots and Systems*, Oct 2007, pp. 839–846.
- [22] F. Aghili, E. Dupuis, J.-C. Piedbœuf, and J. de Carufel, “Hardware-in-the-loop simulations of robots performing contact tasks,” in *International Symposium on Artificial Intelligence and Robotics & Automation in Space: i-SAIRAS*, M. Perry, Ed. Noordwijk, The Netherlands: ESA Publication Division, 1999, pp. 583–588.
- [23] F. Aghili, “A zero-g emulating testbed for spacecraft control systems,” US Patent Application, 11/019,569.
- [24] M. Doyon, J.-C. Piedbœuf, F. Aghili, Y. Gonthier, and E. Martin, “The SPDM task verification facility: On the dynamic emulation in one-g environment using hardware-in-the-loop simulation,” in *Proc. of The 7th International Symposium on Artificial Intelligence and Robotics & Automation in Space: i-SAIRAS*, Nara, Japan, May 19–23 2003.
- [25] J.-C. Piedbœuf, F. Aghili, M. Doyon, and E. Martin, “Dynamic emulation of space robot in one-g environment using hardware-in-loop simulation,” in *CISM-IFTToMM Symposium on Robotics Design, Dynamics and Control*, Italy, July 3–6 2002.
- [26] F. Aghili and J.-C. Piedbœuf, “Contact dynamics emulation for hardware-in-loop simulation of robots interacting with environment,” in *IEEE International Conference on Robotics & Automation*, Washington, USA, May 11–15 2002, pp. 534–529.
- [27] F. Aghili and K. Parsa, “A reconfigurable robot with lockable cylindrical joints,” *IEEE Trans. on Robotics*, vol. 25, no. 4, pp. 785–797, August 2009.
- [28] F. Aghili and C.-Y. Su, “Reconfigurable space manipulators for in-orbit servicing and space exploration,” in *International Symposium on Artificial Intelligence, Robotics and Automation in Space i-SAIRAS*, Turin, Italy, Sep. 4–6 2012.
- [29] B. Bachofer and L. Seaman, “Air bearing dynamic testing—one arc second accuracy,” *AIAA paper*, pp. 64–205, 1964.

- [30] J. E. Colebank, R. D. Jones, G. R. Nagy, R. D. Pllak, and D. R. Mannebach, "SIMSAT: A satellite simulator and experimental test bed for air force research," in *AIAA Paper*, Sep. 1999, pp. 99–44.
- [31] D. Miller, A. Saenz-Otero, J. Wertz, A. Chen, G. Berkowski, C. Brodel, S. Carlson, D. Carpenter, S. Chen, S. Cheng, D. Feller, S. Jackson, B. Pitts, F. Perez, J. Szuminiski, and S. Shell, "SPHERES: A testbed for long duration satellite formation flying in micro-gravity conditions," in *Proceedings of the AAS/AIAA Space Flight Mechanics Meeting*, San Diego, CA, 2000, pp. 167–179.
- [32] M. A. Peck, L. Miller, A. R. Cavender, M. Gonzalez, and T. Hintz, "An airbearing-based testbed for momentum-control systems and spacecraft line of sight," *American Astronautical Society, ASS*, pp. 3–127, Feb. 2003.
- [33] M. Bacic, "On hardware-in-the-loop simulation," in *IEEE Conference on Decision and Control*, Seville, Spain, Dec. 2005, pp. 3194–3198.
- [34] Y. Sato, A. Ejiri, Y. Iida, S. Kanda, T. Maruyama, T. Uchiyama, and H. Fujii, "Micro-g emulation system using constant-tension suspension for a space manipulator," in *IEEE Int. Conference on Robotics and Automation*, Sacramento, CA, Apr. 1991, pp. 1893–1900.
- [35] F. Aghili and C. Y. Su, "Robust relative navigation by integration of icp and adaptive kalman filter using laser scanner and imu," *IEEE/ASME Transactions on Mechatronics*, vol. 21, no. 4, pp. 2015–2026, Aug 2016.
- [36] S. Dubowsky, W. Durfee, A. Kulinski, U. Müller, I. Paul, and J. Pennington, "The design and implementation of a laboratory test bed for space robotics: The ves mod II," in *ASME Conf. DE-Vol. 72, Robotics: Kinematics, Dynamics and Control*, 1994, pp. 99–108.
- [37] F. Aghili, "Automated rendezvous & docking (AR&D) without impact using a reliable 3d vision system," in *AIAA Guidance, Navigation and Control Conference*, Toronto, Canada, August 2010.
- [38] T. Akima, S. Tarao, and M. Uchiyama, "Hybrid micro-gravity simulator consisting of a high-speed parallelrobot," in *IEEE Int. Conference on Robotics and Automation*, Detroit, Michigan, May 1999, pp. 901–906.
- [39] F. Aghili, "A mechatronic testbed for revolute-joint prototypes of a manipulator," *IEEE Trans. on Robotics*, vol. 22, no. 6, pp. 1265–1273, Dec. 2006.
- [40] S. Tarao, E. Inohira, and M. Uchiyama, "Motion simulation using a high-speed parallel link mechanism," in *The 2000 IEEE/RSJ Int. Conf. On Intelligent Robots and Systems*, Takamatsu, Japan, 2000.
- [41] F. Aghili, "Impedance control of manipulators carrying heavy payload for spacecraft rendezvous & docking simulator," in *ASME Mechanisms and Robotics Conference*, San Diego, CA, September 2009.

- [42] K. Yoshida, H. Nakanishi, H. Ueno, N. Inaba, T. Nishimaki, and M. Oda, “Dynamics, control and impedance matching for robotics capture of non-cooperative satellite,” *Journal of Advanced Robotics*, vol. 18, no. 2, pp. 175–198, 2004.
- [43] F. Aghili, “A mechatronics testbed for manipulator joints,” in *IEEE Int. Conference on Robotics & Automation*, Orlando, Florida, May 2006, pp. 2188–2194.
- [44] R. Krenn and B. Schäfer, “Limitations of hardware-in-the-loop simulations of space robotics dynamics using industrial robots,” M. Perry, Ed. Noordwijk, The Netherland: ESA Publication Division, 1999, pp. 681–686.
- [45] S. Ananthakrishnan, R. Teders, and K. Alder, “Role of estimation in real-time contact dynamics enhancement of space station engineering facility,” *IEEE Robotics & Automation Magazine*, no. 3, pp. 20–28, Sep. 1996.
- [46] F. Aghili, “A zero-g emulating testbed for spacecraft control systems,” Canadian Patent 2,521,554.
- [47] F. Aghili, “Robust impedance-matching of manipulators interacting with uncertain environments: Application to task verification of the space station’s dexterous manipulator,” *IEEE/ASME Transactions on Mechatronics*, vol. 24, no. 4, pp. 1565–1576, Aug 2019.
- [48] M. W. Spong and M. Vidyasagar, *Robot Dynamics and Control*. New York, NY: Wiley, 1989.
- [49] C. Canudas de Wit, B. Siciliano, and G. Bastin, Eds., *Theory of Robot Control*. London, Great Britain: Springer, 1996.
- [50] F. Aghili, “Robust impedance control of manipulators carrying heavy payload,” *ASME Journal of Dynamic Systems, Measurements, and Control*, vol. 132, September 2010.
- [51] H. K. Khalil, *Nonlinear Systems*. New-York: Macmillan Publishing Company, 1992.
- [52] *Multi-Axis Force/Torque Sensor, 2007 Catalog*, ATI Industrial Automation, 2007.
- [53] G. C. White and X. Yangsheng, “An active vertical-direction gravity compensation system,” *IEEE Trans. on Instrumentation & Measurement*, vol. 43, no. 6, pp. 786–792, 1994.
- [54] T. Rahman, R. Ramanathan, R. Seliktar, and W. Harwin, “A simple technique to passively gravity-balance articulated mechanisms,” *ASME Journal of Mechanical Design*, vol. 117, no. 4, pp. 655–658, 1995.
- [55] A. Gopalswamy, P. Gupta, and M. Vidyasagar, “A new parallelogram linkage configuration for gravity compensation using torsional springs,” in *IEEE Int. Conference on Robotics & Automation*, May 1992, pp. 664–669.
- [56] N. Ulrich and V. Kumar, “Passive mechanical gravity compensation for robot manipulators,” in *IEEE Int. Conference on Robotics & Automation*, 1991, pp. 1536–1541.